Supporting Information

PtIrFeCoNiMo High-entropy Alloy Nanodendrites for Boosting Alkaline Hydrogen Oxidation Performance

Xiaolong Ma,[a] Shuang Zhang, [a] Yaojiang Zhou, [a] Wenli Lei,[a] Yueming Zhai, [b] Yuanmeng Zhao*[a] and Changsheng Shan*[a]

[a]Collaborative Innovation Center for Advanced Organic Chemical Materials Co-constructed by the Province and Ministry, Ministry of Education Key Laboratory for the Synthesis and Application of Organic Functional Molecules, College of Chemistry and Chemical Engineering, Hubei University, Wuhan 430062, P. R. China.

[b]The Institute for Advanced Studies (IAS), Wuhan University, Wuhan 430072, P. R. China

*E-mail: ymzhao@hubu.edu.cn; csshan@hubu.edu.cn

Experimental Section

Materials. Platinum acetylacetonate (Pt(acac)$_2$, 99%), iridium acetylacetonate (Ir(acac)$_3$, 98%), iron acetylacetonate (Fe(acac)$_3$, 98%), cobalt acetylacetonate (Co(acac)$_3$, ≥99%), nickel acetylacetonate (Ni(acac)$_2$, 95%), Hexadecyltrimethylammonium chloride (CTAC, 96%), oleylamine (OAm, ≥80%) and 1-octadecene (ODE, 98%) were purchased from Aladdin. Molybdenum hexacarbonyl (Mo(CO)$_6$, 98%) was purchased from Strem Chemicals Inc. Nafion solution (5%) was purchased from Sigma-Aldrich. Potassium hydroxide (KOH, 85%), ethanol (C$_2$H$_6$O), and cyclohexane (C$_6$H$_{12}$) were purchased from Sinopharm Chemical Reagent Co., Ltd. Commercial Pt/C for comparison was achieved from Johnson Matthey. The deionized water in the experiment is ultrapure (18.25 MΩ·cm)

Fabrication of PtIrFeCoNiMo nanodendrites (HEA NDs). In a typical synthesis of PtIrFeCoNiMo HEA NDs, Pt(acac)$_2$ (10 mg), Ir(acac)$_3$ (12.2 mg), Ni(acac)$_2$ (6.4 mg), Fe(acac)$_3$ (8.8 mg), Co(acac)$_3$ (8.9 mg) and 80 mg CTAC were added into a two-necked round-bottom flask containing 20 mL of a mixture of OAm/ODE (v/v = 4:1). To obtain a homogeneous mixture, the mixture was sonicated continuously for 2 h. Then, the two-necked round-bottom flask was heated up to 110 °C at 5 °C/min. After that, Mo(CO)$_6$ (14 mg) was added rapidly, and the temperature was further heated up to 220°C and maintained at this temperature for another 5 h. After cooling, the products were collected by centrifugation at 9000 rpm for 10 min and washed with ethanol/cyclohexane (v/v = 3:1) for three times. After dried in vacuum, the PtIrFeCoNiMo HEA NDs were obtained. For the synthesis of HEA NPs, all of the

conditions are similar to those of HEA NDs but without adding CTAC. Besides, for probing the influence of stoichiometry variations on the alkaline HOR activities, we changed the contents of Pt as an example. The PtIrFeCoNiMo HEA NDs with different Pt contents were synthesized by the same procedure except adding different amount of $Pt(acac)_2$, the elementary compositions of the obtained materials were acquired by ICP-OES tests, named as $Pt_{38}Ir_{22}Fe_{13}Co_3Ni_{18}Mo_6$ with 12.5 mg $Pt(acac)_2$ and $Pt_{32}Ir_{23}Fe_8Co_4Ni_{26}Mo_7$ with 7.5 mg $Pt(acac)_2$, respectively.

Material characterization. The X-ray diffraction (XRD) patterns were recorded on a Bruker D8 Advance diffractometer with Cu Kα radiation. The transmission electron microscopy (TEM) and high-resolution transmission electron microscopy (HRTEM) and scanning transmission electron microscopy (STEM) images, as well as energy dispersive X-ray spectroscopy (EDS) data were carried out by a JEOL JEM-2100F field emission transmission electron microscope equipped with an EDS spectrometer operated at 200 kV. The X-ray photoelectron spectroscopy (XPS) was collected from a Thermo Fisher Scientific ESCALAB 250Xi XPS system, and the binding energy of the C1s peak at 284.8 eV was taken as a reference. The inductively coupled plasma optical emission spectrometer (ICP-OES) measurements were conducted on an Agilent ICP-OES 725 analyzer.

Preparation of working electrodes. The as-synthesized samples and a certain amount of XC-72 carbon black were mixed in 20 mL ethanol and stirred under N_2 flow at room temperature for more than 12 hours. Finally, the black mixture was transferred into a centrifuge tube and centrifuged. Then, the solution after centrifugation was

poured out and the obtained precipitate was dried under vacuum to obtain HEA NDs/C or other control catalysts.

The 4 mg as-synthesized catalysts were dispersed into a 2 mL of isopropyl alcohol containing 0.025 wt.% Nafion and ultrasonicated for more than 30 min to form a homogeneous ink. Then the catalyst ink with the concentration of 2 mg mL^{-1} was obtained. The glassy carbon electrode (GCE) with a diameter of 5 mm was polished with 0.05 μm gamma alumina powder and rinsed with ultrapure water and ethanol to obtain a neat surface. When the GCE was dried under air naturally, 6 μL ink was drop-casted on the surface of the GCE and dried in the air before any electrochemical measurements.

Electrochemical measurements. Electrochemical measurements were conducted at CHI760 electrochemical workstation with a conventional three-electrode system. Catalysts-modified GCE, Hg/HgO electrode and a graphite rod were used as the working electrode, reference electrode and counter electrode, respectively. All potentials in this paper are converted to the reversible hydrogen electrode (RHE) based on the following equation: E (V vs. RHE) = E (V vs. Hg/HgO) + 0.059*pH (V) + 0.157 (V). The electrolyte used for the HOR tests is 0.1 M KOH solution.

Before HOR tests, cyclic voltammetry (CV) ranging from ~0.02 to 0.72 V was conducted in an Ar-saturated 0.1 M KOH solution to obtain the steady voltammetry curves with the scanning rate of 50 mV s^{-1}. Then, HOR polarization curves were performed by using a rotation disk electrode (RDE) with a rotation speed of 1600 rpm

and the potential from -0.08 V to 0.72 V at a scan rate of 10 mV s^{-1} in H$_2$-saturated

electrolyte for HOR. Electrochemical impedance spectra (EIS) tests were conducted

with the AC impedance spectra from 100 kHz to 1 Hz and a voltage perturbation of 10

mV. The real part of the resistance at 1 kHz was taken as the uncompensated resistance

(R_u) and was used to obtain the iR-free potential (E$_{iR\text{-}free}$) according to the following

equation: $E_{iR-free} = E - iR_u$, where E is the measured potential and i is the

corresponding current. Kinetic current density (j^k) could be deduced from the

Koutecky-Levich equation: $\dfrac{1}{j} = \dfrac{1}{j^k} + \dfrac{i}{j^d} = \dfrac{1}{j^k} + \dfrac{1}{Bc_0\omega^{1/2}}$, where j, j^d, B, c_0, and ω are the

measured current density, the diffusion limited current density, the Levich constant, the

solubility of H$_2$ and the speed of the rotating speed, respectively. Exchange current

density (j^0), often used to evaluate the intrinsic activity of a catalyst, could be deduced

from the Butler-Volmer equation: $j^k = j^0\left(e^{\frac{\alpha F}{RT}\eta} - e^{\frac{-(1-\alpha)F}{RT}\eta}\right)$, where α, R, T, and η

represent the transfer coefficient, the universal gas constant (8.314 J mol^{-1} K^{-1}), the

operating temperature (303 K in this work), and the overpotential, respectively. The

value of j^0 can also be obtained from the micro-polarization region, which is the region

where only several millivolts deviate from the equilibrium potential. In this narrow

region, the diffusional component can be ignored and the kinetic current can be

represented by the measured current (j). The Butler-Volmer equation can be simplified

to equation: $j = j^0\dfrac{F}{RT}\eta$. The ECSAs for HEA NDs, HEA NPs and commercial Pt/C

were determined by CO stripping, which was conducted by keeping the electrode

potential at 0.1 V for 10 min in 0.1 M KOH solution with 99.99% CO for CO adsorbed

on metal surface, followed by Ar purging for another 30 min to remove residual CO in the electrolyte. The CO stripping current was obtained via CV in a potential region from 0 to 1.0 V at a sweep rate of 20 mV s^{-1}. The first CV represents the stripping of a monolayer of CO. The second CV represents the background. The ECSAs were calculated from the charge of the first CV by subtracting the second CV corresponding to a charge density of 420 μC cm^{-2}. Accelerated durability tests (ADT) of HOR for all samples were measured between their CV potential windows at the scan rate of 500 mV s^{-1} in Ar-saturated 0.1 M KOH electrolyte for 1000 cycles. Then, the HOR polarization curve was recorded in H$_2$-saturated 0.1 M KOH electrolyte at 10 mV s^{-1} from -0.08 to 0.72 V for the comparison with the initial curve before 1000 CVs. The chronoamperometry method was also used to assess the catalyst's stability at 100 mV vs. RHE in an H$_2$-saturated 0.1 M KOH solution. CO-tolerance test was performed using the same electrochemical measurements of HOR test. The linear sweep voltammetry (LSV) curves of the samples were carried out in 0.1 M KOH saturated with H$_2$ or H$_2$ containing 100 ppm CO at the rotation rate of 1600 rpm and the potential was ranged from - 0.08 V to 0.72 V at a scan rate of 10 mV s^{-1}.

Thermodynamic Calculations. The value of mixed entropy of mixing (ΔS_{mix}) was calculated based on the atomic percent of each metal element in the material. According to Boltzmann's hypothesis, the ΔS_{mix} can be defined as follows.[1,2]

$$\Delta S_{mix} = - R \sum_{i=1}^{n} x_i In x_i$$

where R is the gas constant, x_i the molar fraction of the i_{th} element, and n denotes the

number of elemental components in the alloys. According to the calculation of the ΔS_{mix}, alloys can be divided into low ($\Delta S_{mix} < 8.314$ J mol^{-1} kg^{-1}), medium (8.314 J mol^{-1} kg^{-1} $\leq \Delta S_{mix} \leq 12.55$ J mol^{-1} kg^{-1}), and HEAs ($\Delta S_{mix} > 12.55$ J mol^{-1} kg^{-1}).[3,4]

Density Functional Theory (DFT) calculations. The randomly arranged sites of the disordered HEA was simulated by generating the special quasi-random structure (SQS) from the "mcsqs" utility of the Alloy Theoretic Automated Toolkit (ATAT) code, as SQS represent the best periodic approximation to the true disordered state.[5,6] Such quasi-random structures have been successful in reproducing catalytic and other properties of HEAs. The 4 ⅹ 4 ⅹ 1 supercell of Pt (111) surface with four layers containing 64 atoms was taken for generating the HEA structure with the atomic ratio of Pt/Ir/Ni/Fe/Co/Mo = 11:6:4:5:2:4, which is close to the ICP-OES results. Then DFT calculations were performed by CASTEP package to explore the origin of the superior HOR activity of HEA. The generalized gradient approximation functional of the Perdew-Burke-Ernzerhof (PBE) form was used to describe the exchange and correlation interactions.[7] Ultrasoft pseudo-potential was adopted to treat the interactions between ionic cores and valence electrons. The electronic wave functions were expanded on a plane wave basis with a cut-off energy of 400 eV. The optimization convergence criterion was set as 2×10^{-6} eV atom^{-1} in energy. And for both of HEA (111) and Pt (111) slabs, a vacuum region of 15Å in the z axis to avoid the interactions between neighboring images was chosen, and the bottom two layers were kept fixed while the topmost two layers and the adsorbates were allowed to relax. The adsorption free energies were determined by the following formula $\Delta G = \Delta E + \Delta ZPE - T\Delta S$, where

ΔE, ΔZPE and ΔS represent the binding energy, zero point energy change and entropy change of the adsorption of adsorbates, respectively.[8] The related zero point energies and entropies of H_2, H_2O, H* and OH* are from previous literatures.[8]
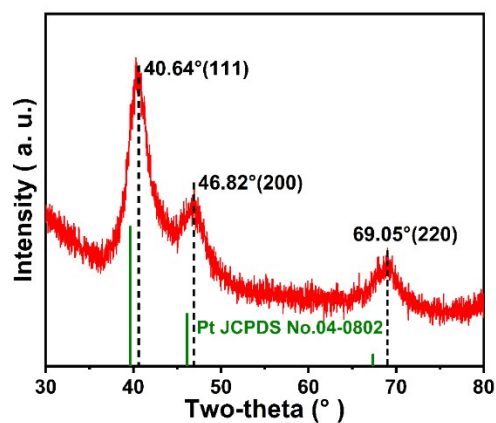
Fig. S1 XRD pattern of HEA NDs/C.
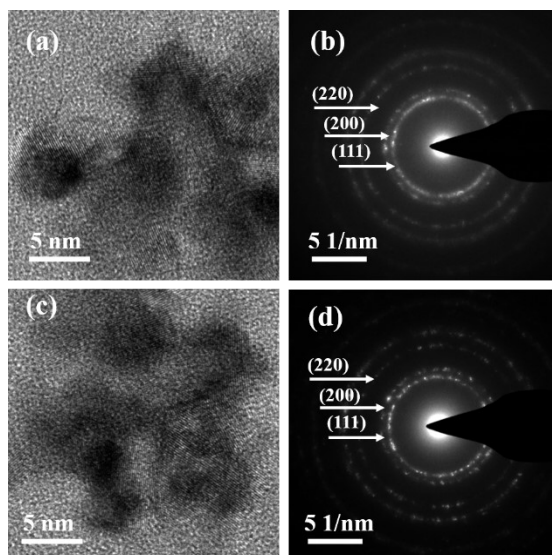
Fig. S2 (a, c) HRTEM images and (b, d) corresponding SAED patterns for HEA NDs.
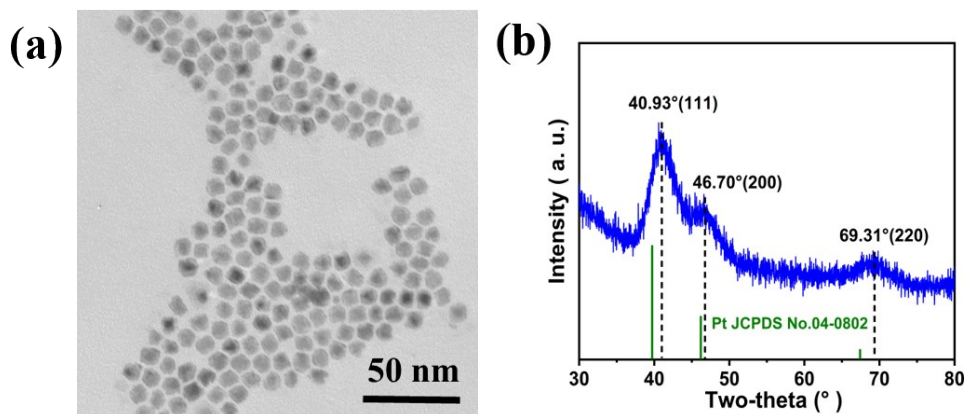
Fig. S3 (a)TEM image of HEA NPs. (b) XRD pattern of HEA NPs/C.
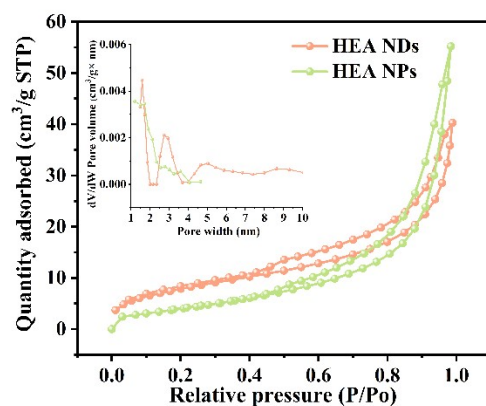
Fig. S4 Nitrogen adsorption–desorption isotherm of HEA NDs and HEA NPs. Inset: The distribution of pore size of HEA NDs and HEA NPs.
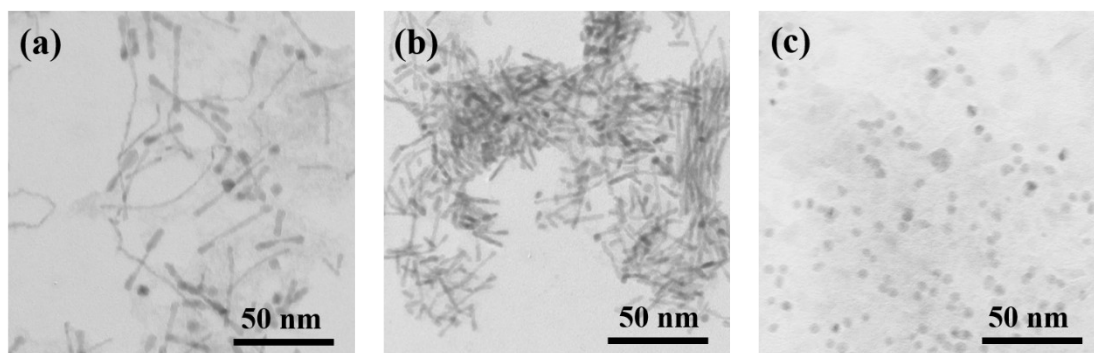
Fig. S5 TEM images of HEA nanomaterials with different volume ratios of OAM and ODE of (a) 2.5:2.5, (b) 1:4 and (c) 0:5.
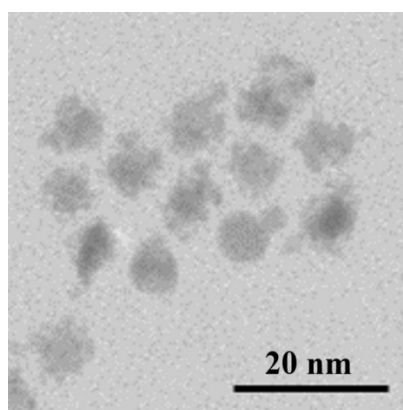
Fig. S6 Magnified TEM image of HEA NDs at reaction time of 0.5 h.
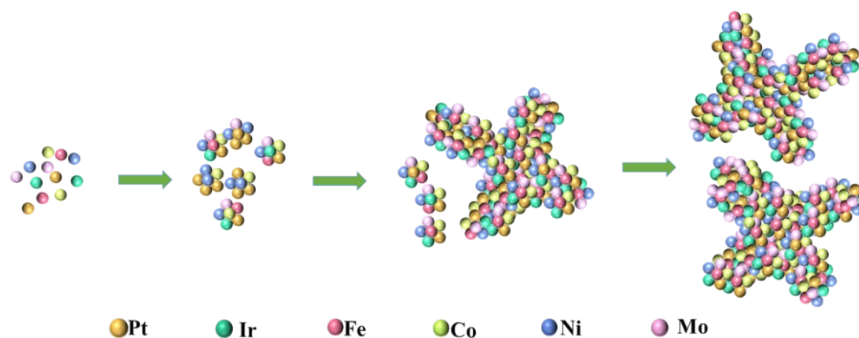
Fig. S7 Illustration of the assembly process of HEA NDs.
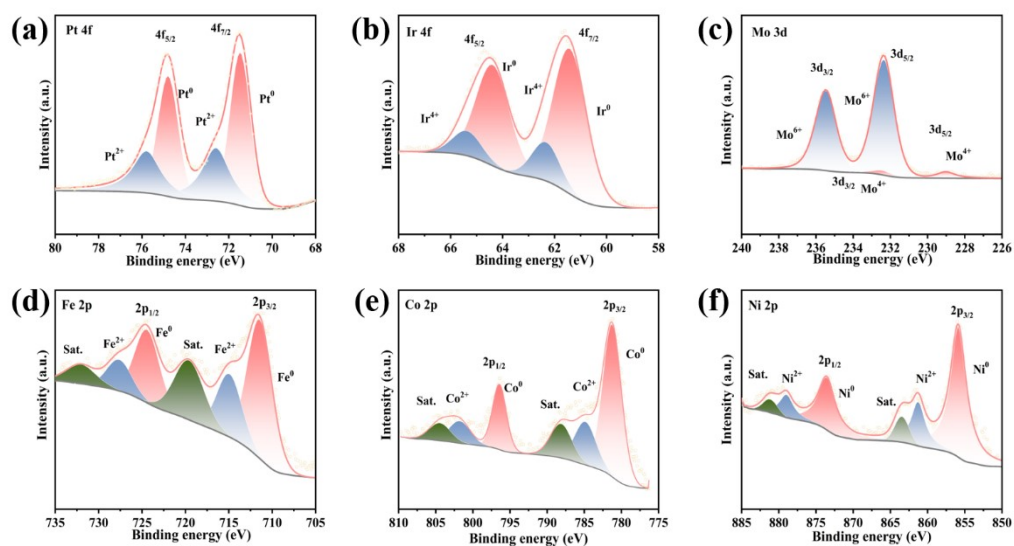
Fig. S8 XPS spectra of Pt 4f (a), Ir 4f (b), Mo 3d (c), Fe 2p (d), Co 2p (e) and Ni 2p (f).

Fig. S9 High-resolution XPS spectra of O 1s for HEA NDs at different etching time (0, 1, 2, 3 and 4 minutes).

Fig. S10 High-resolution XPS spectra of Pt 4f (a), Ir 4f (b), Mo 3d (c), Fe 2p (d), Co 2p (e) and Ni 2p (f) for HEA NDs at different etching time (0, 1, 2, 3 and 4 minutes).
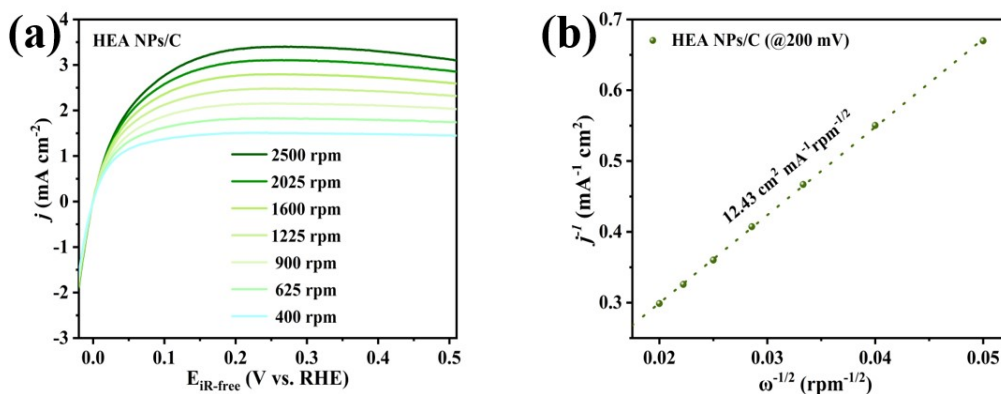
Fig. S11 (a) HOR polarization curves of HEA NPs/C in H_2-saturated 0.1 M KOH solution at the rotating speeds varied from 2500 to 400 rpm. (b) The corresponding Koutecky-Levich plots of HEA NPs/C (@200 mV).
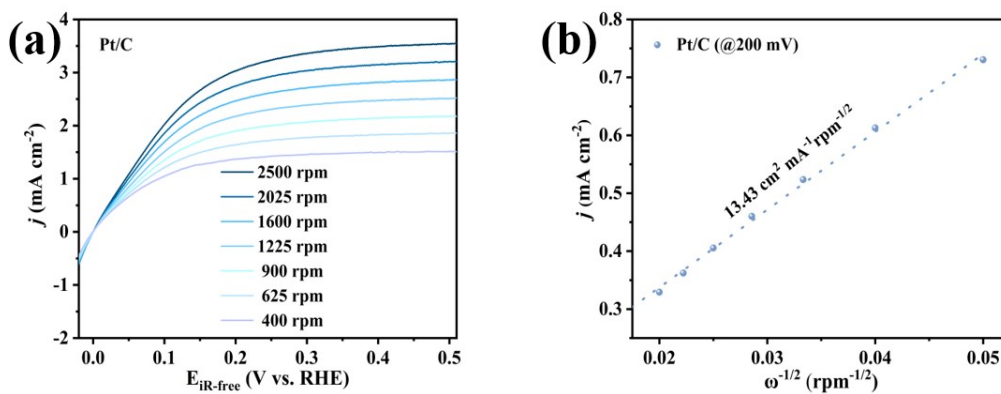
Fig. S12 (a) HOR polarization curves of Pt/C in H_2-saturated 0.1 M KOH solution at the rotating speeds varied from 2500 to 400 rpm. (b) The corresponding Koutecky-Levich plots of Pt/C (@200 mV).
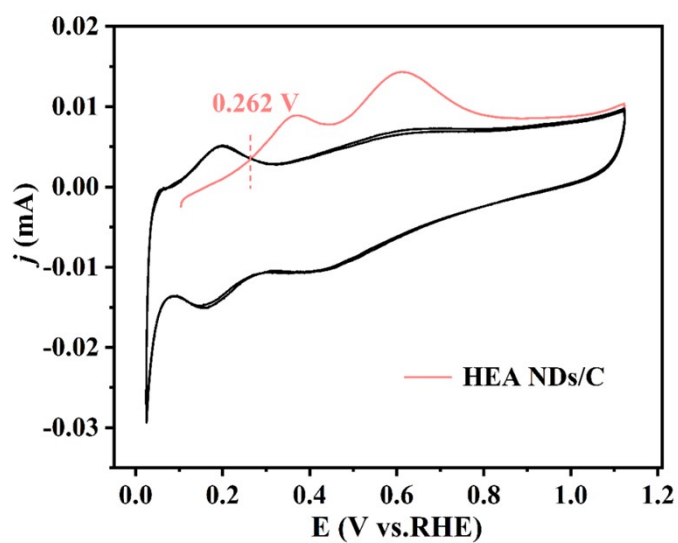
Fig. S13 CO-stripping curve of HEA NDs/C in 0.1 M KOH solution at a scan rate of
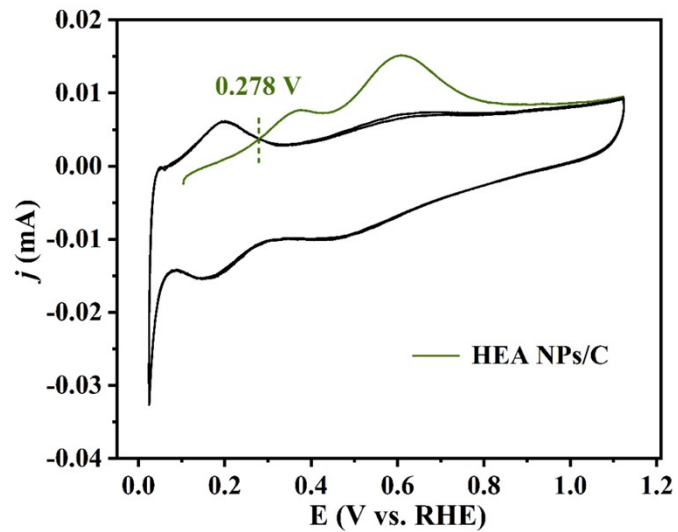
5 mV s^{-1}.

Fig S14 CO-stripping curve of HEA NPs/C in 0.1 M KOH solution at a scan rate of 5
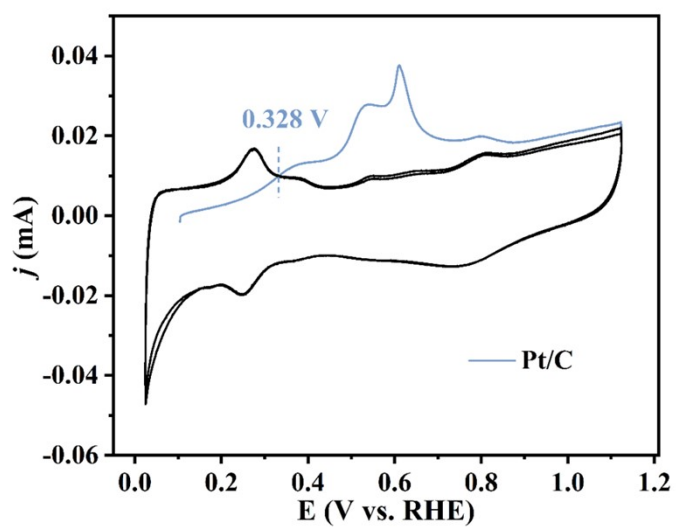
mV s^{-1}.

Fig. S15 CO-stripping curve of commercial Pt/C in 0.1 M KOH solution at a scan rate of 5 mV s^{-1}.
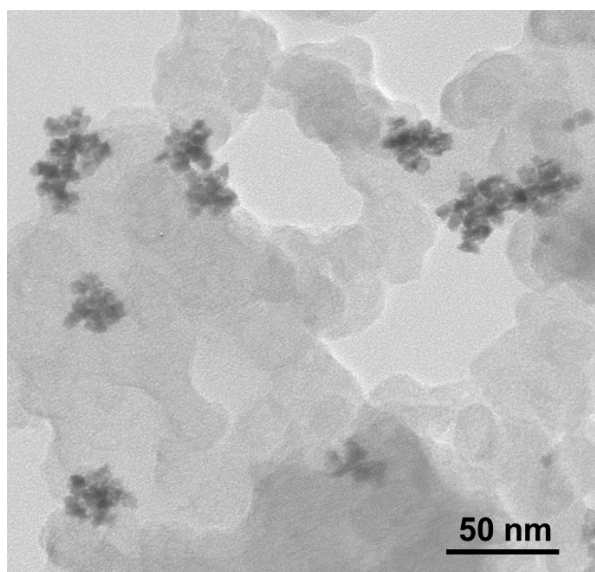
Fig. S16 TEM image of HEA NDs/C after HOR stability test in Ar-saturated 0.1 M KOH solution.
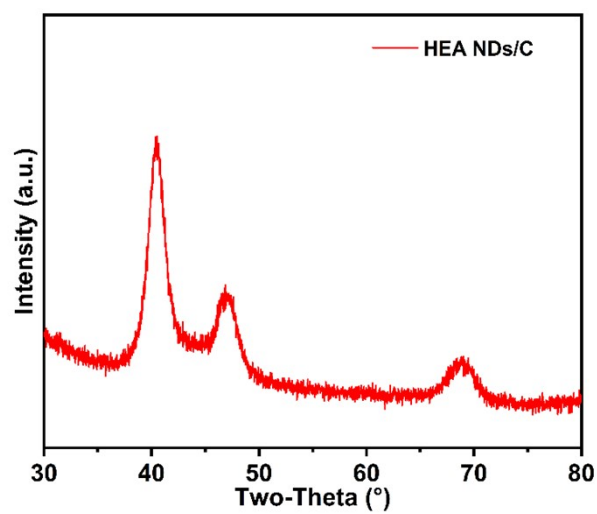
Fig. S17 XRD pattern of HEA NDs/C after HOR ADT in Ar-saturated 0.1 M KOH solution.
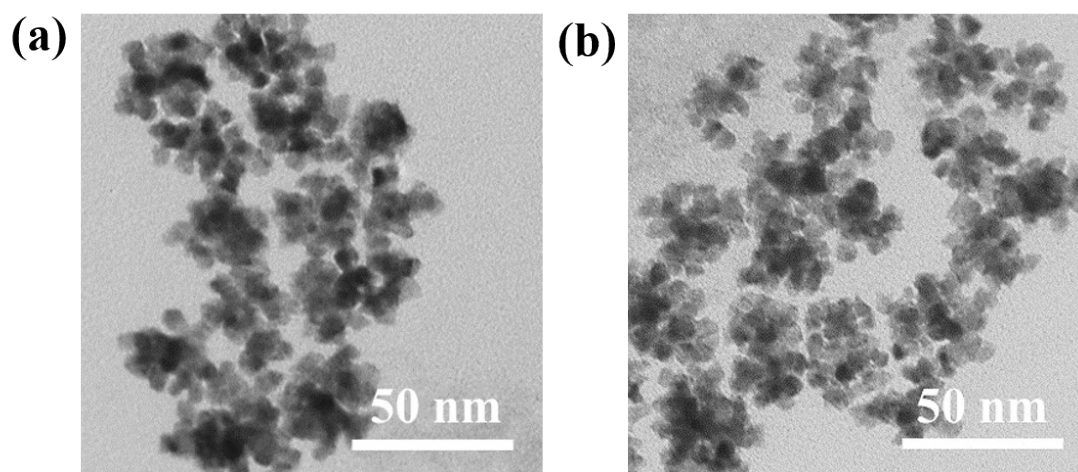
Fig. S18 TEM images of (a) $Pt_{38}Ir_{22}Fe_{13}Co_3Ni_{18}Mo_6$ and (b) $Pt_{32}Ir_{23}Fe_8Co_4Ni_{26}Mo_7$ HEA NDs.
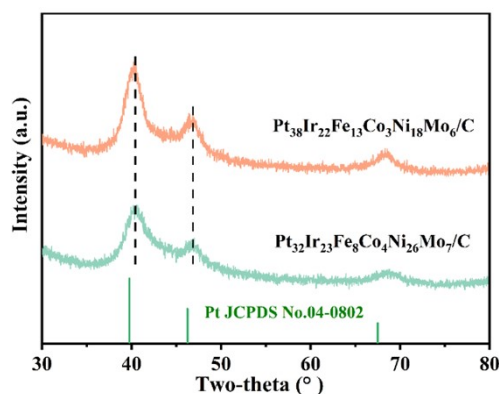
Fig. S19 XRD patterns of $Pt_{38}Ir_{22}Fe_{13}Co_3Ni_{18}Mo_6/C$ and $Pt_{32}Ir_{23}Fe_8Co_4Ni_{26}Mo_7/C$.
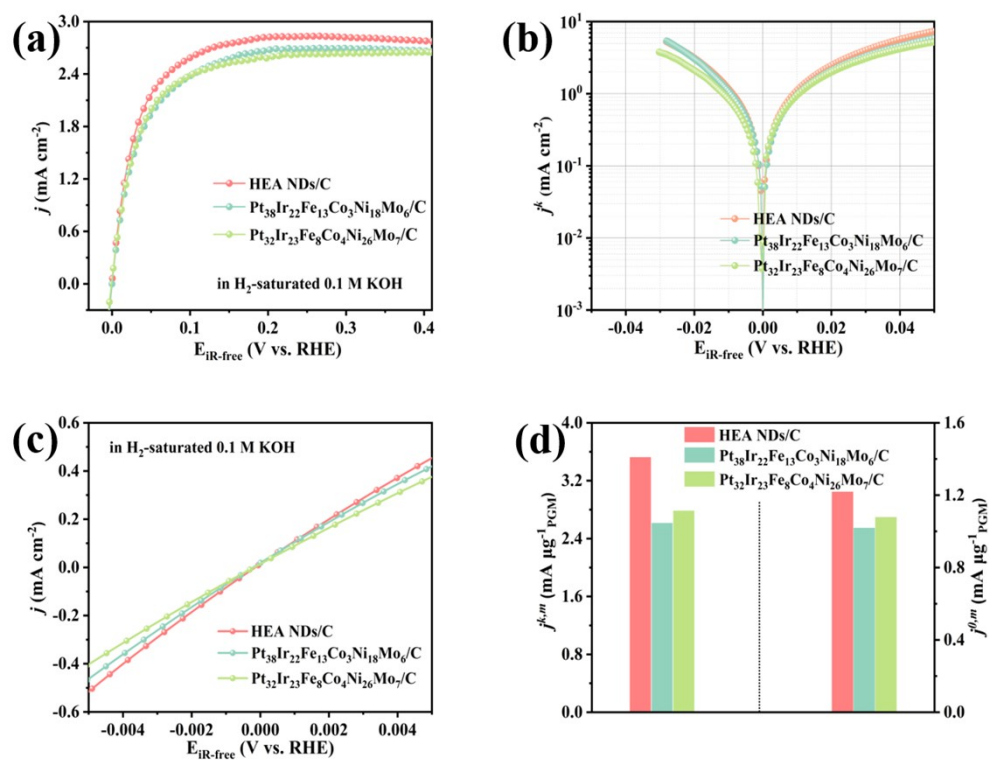
Fig. S20 (a) HOR polarization curves in H_2-saturated 0.1 M KOH solution. (b) Linear current potential region around the equilibrium potential. (c) Tafel plots of the HER/HOR kinetic current density. (d) Exchange current densities normalized by metal mass of HEA NDs/C, $Pt_{38}Ir_{22}Fe_{13}Co_3Ni_{18}Mo_6/C$ and $Pt_{32}Ir_{23}Fe_8Co_4Ni_{26}Mo_7/C$.
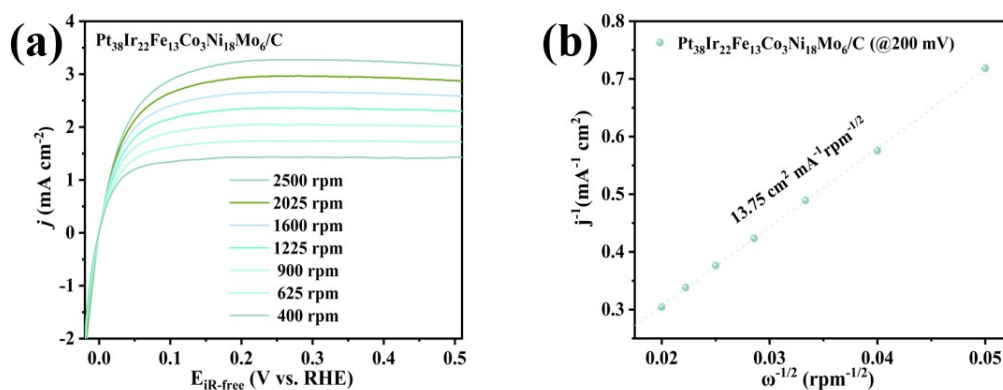
Fig. S21 (a) HOR polarization curves of $Pt_{38}Ir_{22}Fe_{13}Co_3Ni_{18}Mo_6$/C in H_2-saturated 0.1 M KOH solution at the rotating speeds varied from 2500 to 400 rpm. (b) The corresponding Koutecky-Levich plots of Pt/C (@200 mV).
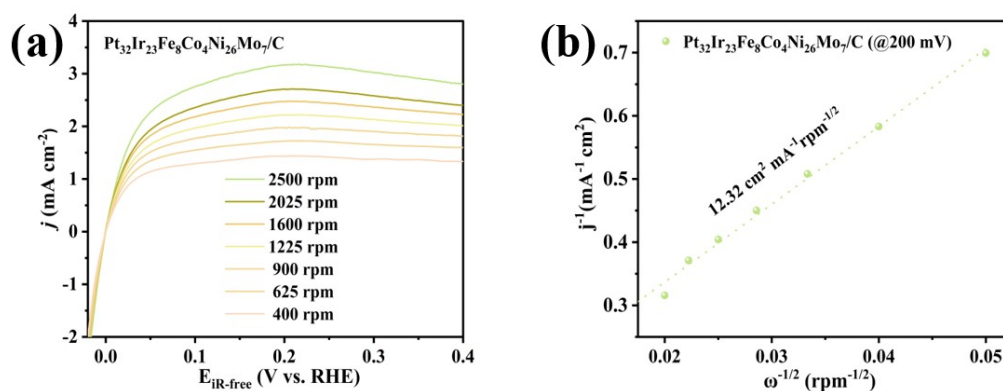
Fig. S22 (a) HOR polarization curves of $Pt_{32}Ir_{23}Fe_8Co_4Ni_{26}Mo_7$/C in H_2-saturated 0.1 M KOH solution at the rotating speeds varied from 2500 to 400 rpm. (b) The corresponding Koutecky-Levich plots of Pt/C (@200 mV).
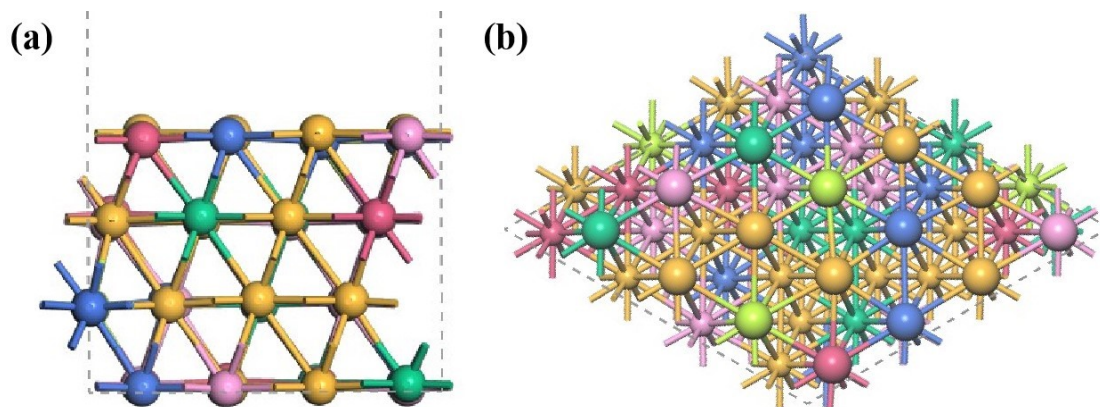
Fig. S23 The side view (a) and top view (b) of PtIrFeCoNiMo HEA (111) surface. The orange, pink, purple blue, yellowish green, cyan and rose red balls represent Pt, Ir, Fe, Co, Ni and Mo atoms, respectively.
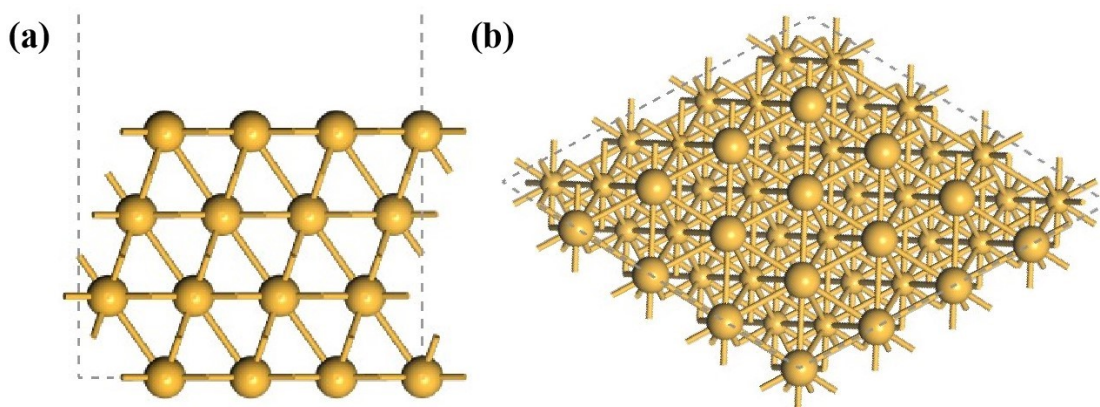
Fig. S24 The side view (a) and top view (b) of Pt (111) surface.
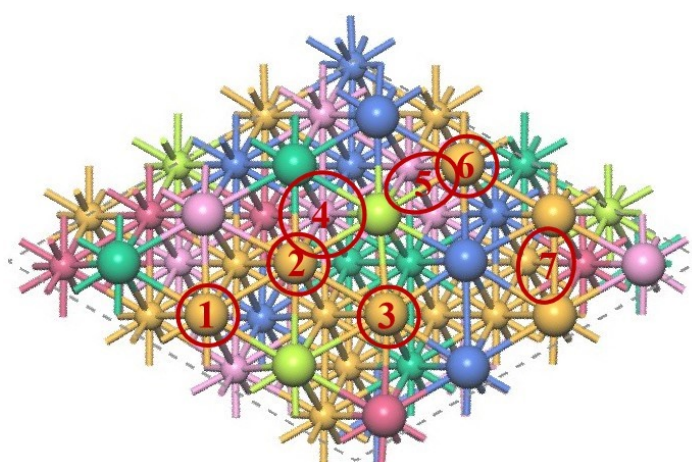
Fig. S25 The different H adsorption sites on PtIrFeCoNiMo HEA (111) surface after geometry optimizations.
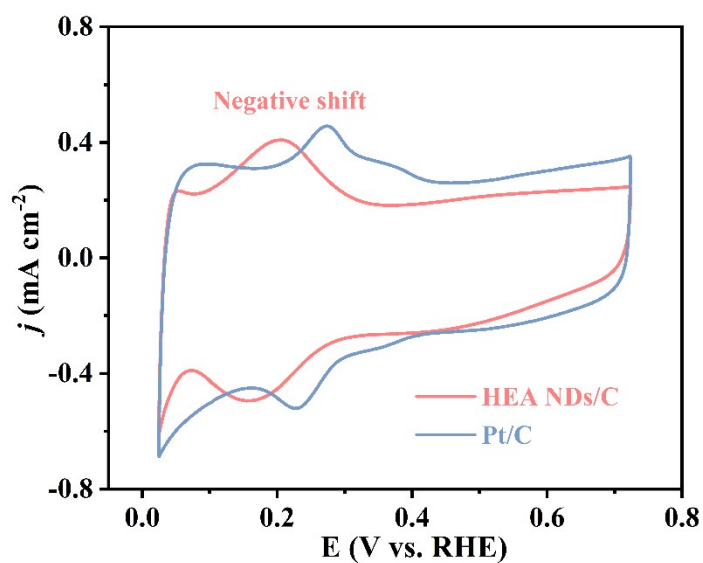
Fig. S26 CV curves of HEA NDs/C and Pt/C conducted in Ar-saturated 0.1 M KOH solution at a scan rate of 50 mV s^{-1}.
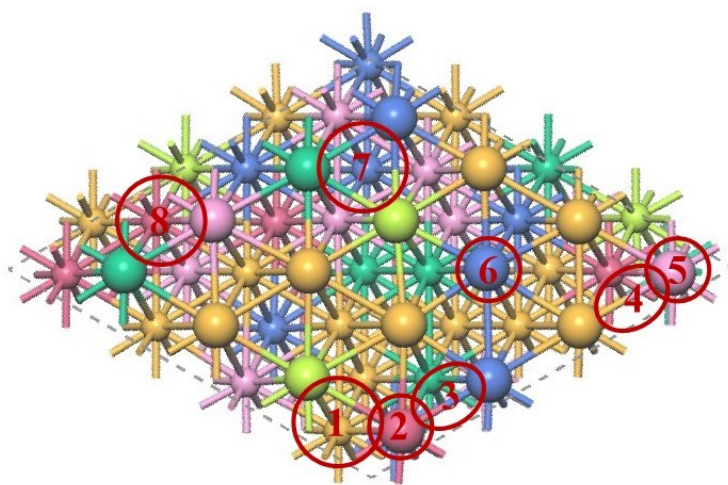
Fig. S27 The different OH adsorption sites on PtIrFeCoNiMo HEA (111) surface after geometry optimizations.
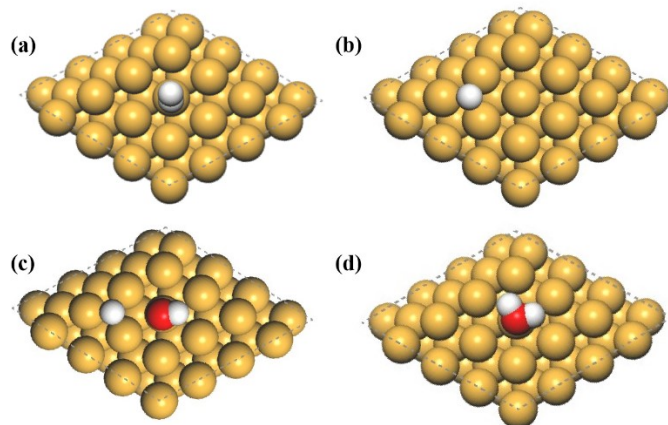
Fig. S28 The optimal theoretical structures of H*, H*+OH* and H$_2$O* on Pt (111) surface.

Table S1. ICP-OES results of the contents of Pt, Ir, Fe, Co, Ni and Mo in HEA.

		Pt	Ir	Fe	Co	Ni	Mo
HEA NDs/C	Atomic ratio	34.97	21.11	15.50	5.99	16.80	5.63
	Wt(%)	3.67	2.18	0.47	0.19	0.53	0.29
Pt$_{38}$Ir$_{22}$Fe$_{13}$Co$_3$Ni$_{18}$Mo$_6$/C	Atomic ratio	37.95	22.08	13.26	3.33	17.73	5.66
	Wt(%)	4.76	2.73	0.48	0.13	0.67	0.35
Pt$_{32}$Ir$_{23}$Fe$_8$Co$_4$Ni$_{26}$Mo$_7$/C	Atomic ratio	32.00	23.13	8.25	3.76	26.34	6.52
	Wt(%)	3.10	2.21	0.23	0.11	0.77	0.31
HEA NPs/C	Atomic ratio	27.99	17.06	12.49	13.31	16.36	12.78
	Wt(%)	3.23	2.99	0.41	0.47	0.57	0.72

Table S2. The data of catalysts in this work for HOR activity.

Catalyst	Loading	ESCA	Butler-Volmer fitting			Micro-polarization	
			$j^{0,s}$	$j^{0,m}$	$j^{k,m}$ @50 mV	$j^{0,s}$	$j^{0,m}$
	$\mu g_{(PGM)}/cm^2$	$m^2 g^{-1}_{PGM}$	$mA\ cm^{-2}_{ECSA}$	$mA\ \mu g^{-1}_{PGM}$	$mA\ \mu g^{-1}_{PGM}$	$mA\ cm^{-2}_{ECSA}$	$mA\ \mu g^{-1}_{PGM}$
HEA NDs/C	2.13	45.29	1.13	1.22	3.53	1.13	1.22
HEA NPs/C	1.98	50.46	0.63	0.82	2.07	0.73	0.95
Pt/C	12.23	55.46	0.51	0.12	0.25	0.50	0.12

Table S3. HOR activities of the reported HOR electrocatalysts in alkaline electrolyte.

Catalyst	Loading $\mu g_{(PGM)}/cm^2$	$j^{0,s}$ mA cm^{-2}_{ECSA}	$j^{0,m}$ mA μg^{-1}_{PGM}	$j^{k,m}$ mA μg^{-1}_{PGM}	Ref.
HEA NDs/C	**2.13**	**1.13**	**1.22**	**3.53@50 mV**	**This work**
HEA-PdNiRuIrRh NPs	6.98	1.19	/	3.247@50 mV	9
PtRhMoIrRu-HEANWs	9.1	/	0.7	5.8@50 mV	10
PtRuNiCoFeMo HEA SNWs	8.8	0.753	/	6.75@50 mV	11
IrNi@Ir	10	0.86	1.22	1.12@50 mV	12
PtMo-CeO$_x$-NAs	10	1.00	0.231	3.49@50 mV	13
PtRu/Mo$_2$C−TaC	13	0.20	0.291	0.403 @25 mV	14
PtRu/C	3.8	0.08	0.266	0.364@25mV	
Ni$_1$Ru$_1$/C(L)	12.5	0.078	0.070	0.224@50 mV	15
20%Pt/C(L)	10.2	0.103	0.064	0.203@50 mV	
0.38CeO$_x$-Pd/C	13	0.118	0.052	/	16
Pt$_2$-Rh NSs	15.3	2.21	/	9.61@50 mV	17
hcp/fcc-Ru	6.57	0.664	/	1.016@50mV	18
Pd$_3$Co@Pt/C	1.87	0.057	0.683	/	19
Pd-Pd$_4$S/ C	/	0.225	0.097	0.037@50 mV	20
Ru-Cr$_1$(OH)$_x$-2.2	60	0.28	/	0.601@50 mV	21
RhMo NSs/C	17.6	/	/	6.96@50 mV	22

References

1 Y. Zhang, Y. J. Zhou, J. P. Lin, G. L. Chen and P. K. Liaw, *Adv. Eng. Mater.,*, 2008, **10**, 534-538.

2 Y.-H. Liu, C.-J. Hsieh, L.-C. Hsu, K.-H. Lin, Y.-C. Hsiao, C.-C. Chi, J.-T. Lin, C.-W. Chang, S.-C. Lin, C.-Y. Wu, J.-Q. Gao, C.-W. Pao, Y.-M. Chang, M.-Y. Lu, S. Zhou and T.-H. Yang, *Sci. Adv.,*, 2023, **9**, eadf9931.

3 X. Chang, M. Zeng, K. Liu and L. Fu, *Adv. Mater.*, 2020, **32**, 1907226.

4   Y. Yao, Q. Dong, A. Brozena, J. Luo, J. Miao, M. Chi, C. Wang, I. G. Kevrekidis, Z. J. Ren, J. Greeley, G. Wang, A. Anapolsky and L. Hu, *Science*, 2022, **376**, eabn3103.

5   A. Zunger, S. H. Wei, L. G. Ferreira and J. E. Bernard, *Phys. Rev. Lett.*, 1990, **65**, 353-356.

6   S. Nellaiappan, N. K. Katiyar, R. Kumar, A. Parui, K. D. Malviya, K. G. Pradeep, A. K. Singh, S. Sharma, C. S. Tiwary and K. Biswas, *ACS Catal.,*, 2020, **10**, 3658-3663.

7   J. P. Perdew, K. Burke and M. Ernzerhof, *Phys. Rev. Lett.*, 1996, **77**, 3865-3868.

8   J. K. Nørskov, T. Bligaard, A. Logadottir, J. R. Kitchin, J. G. Chen, S. Pandelov and U. Stimming, *J. Electrochem. Soc.*, 2005, **152**, J23.

9   Y. Men, D. Wu, Y. Hu, L. Li, P. Li, S. Jia, J. Wang, G. Cheng, S. Chen and W. Luo, *Angew. Chem., Int. Ed.,*, 2023, **62**, e202217976.

10   Y. Sun, W. Zhang, Q. Zhang, Y. Li, L. Gu and S. Guo, *Matter*, 2023, **6**, 193-205.

11   C. Zhan, Y. Xu, L. Bu, H. Zhu, Y. Feng, T. Yang, Y. Zhang, Z. Yang, B. Huang, Q. Shao and X. Huang, *Nat. Commun.*, 2021, **12**, 6261.

12   D. Liu, S. Lu, Y. Xue, Z. Guan, J. Fang, W. Zhu and Z. Zhuang, *Nano Energy*, 2019, **59**, 26-32.

13   P. Wang, H. Cui and C. Wang, *Chem. Eng. J.*, 2022, **429**, 132435.

14   E. R. Hamo, R. K. Singh, J. C. Douglin, S. Chen, M. B. Hassine, E. Carbo-Argibay, S. Lu, H. Wang, P. J. Ferreira, B. A. Rosen and D. R. Dekel, *ACS Catal.,*,

2021, **11**, 932-947.

15   J. Liu, J. Wang, Y. Fo, B. Zhang, C. Molochas, J. Gao, W. Li, X. Cui, X. Zhou, L. Jiang and P. Tsiakaras, *Chem. Eng. J.*, 2023, **454**, 139959.

16   R. K. Singh, E. S. Davydova, J. Douglin, A. O. Godoy, H. Tan, M. Bellini, B. J. Allen, J. Jankovic, H. A. Miller, A. C. Alba-Rubio and D. R. Dekel, *Adv. Funct. Mater.*, 2020, **30**, 2002087.

17   J. Cai, X. Zhang, Z. Lyu, H. Huang, S. Wang, L. Fu, Q. Wang, X.-F. Yu, Z. Xie and S. Xie, *ACS Catal.,*, 2023, **13**, 6974-6982.

18   Y. Li, C. Yang, J. Yue, H. Cong and W. Luo, *Adv. Funct. Mater.*, 2023, **33**, 2211586.

19   T. Zhao, Y. Hu, M. Gong, R. Lin, S. Deng, Y. Lu, X. Liu, Y. Chen, T. Shen, Y. Hu, L. Han, H. Xin, S. Chen and D. Wang, *Nano Energy*, 2020, **74**, 104877.

20   L. Su, Y. Zhao, Y. Jin, Z. Liu, H. Cui and W. Luo, *Adv. Funct. Mater.*, 2022, **32**, 2113047.

21   B. Zhang, B. Zhang, G. Zhao, J. Wang, D. Liu, Y. Chen, L. Xia, M. Gao, Y. Liu, W. Sun and H. Pan, *Nat. Commun.*, 2022, **13**, 5894.

22   J. Zhang, X. Liu, Y. Ji, X. Liu, D. Su, Z. Zhuang, Y.-C. Chang, C.-W. Pao, Q. Shao, Z. Hu and X. Huang, *Nat. Commun.*, 2023, **14**, 1761.